High Power Laser Science and Engineering, (2024), Vol. 12, e95, 9 pages.
doi:10.1017/hpl.2024.82

HIGH POWER LASER SCIENCE AND ENGINEERING

RESEARCH ARTICLE

Watt-level sub-100 fs third near-infrared window laser generated by self-seeded coherent Raman amplification based on erbium-ytterbium co-doped fiber

Jiaxuan Zhang, Jintao Fan, and Minglie Hu

Ultrafast Laser Laboratory, Key Laboratory of Optoelectronic Information Technology, Ministry of Education, School of Precision Instrument and Optoelectronics Engineering, Tianjin University, Tianjin, China

(Received 10 August 2024; revised 1 November 2024; accepted 5 November 2024)

Abstract

In this paper, we prove that the third near-infrared (NIR-III) window high-power laser with wavelength in the range of 1600–1800 nm can be obtained by the coherent Raman fiber amplification technique through theoretical and experimental study. Detailed numerical simulation reveals that the nonlinear dynamics of the Raman fiber amplification in the polarization-maintaining double-clad erbium-ytterbium co-doped fiber is similar to that of the Mamyshev oscillator. Through the spectral filtering effect induced by finite Raman gain, we can obtain a high-quality Raman pulse. According to the theoretical results, we design a simple Raman fiber amplification laser and finally obtain a high-quality watt-level NIR-III window laser pulse in which the central wavelength is about 1650 nm and the pulse width can reach 85 fs. The experimental results correspond to the simulation results. Such nonlinear effect is universal in all kinds of fibers, and we think this technology can provide a great contribution to the development of ultrafast fiber lasers.

Keywords: fiber amplifier; nonlinear optics; Raman scattering; third near-infrared window; ultrafast optics

1. Introduction

The ultrafast fiber laser is usually defined as a mode-locked fiber laser with the pulse width of the order of picoseconds or femtoseconds. Compared with the traditional solid-state laser, it has the advantages of a simple structure, excellent heat dissipation performance and good beam quality. It is an important tool for the study of nonlinear optics and laser technology. With the development of various fiber preparation and laser technologies, the performance parameters of the ultrafast fiber laser have been improved and it has been widely used in the fields of laser micromachining[1], biomedicine[2] and optical communication[3]. Ultrafast fiber lasers of different wavebands are suitable for different fields. The third near-infrared (NIR-III) window is the laser window located in the wavelength range of 1600–1800 nm. This band is not only at the trough between the absorption peaks of water molecules, but also at the peak of the absorption peaks of fat and collagen; in addition, it also covers the absorption peak window of C-H covalent bonds, which has been widely used in the fields of laser medicine[4], biological imaging[5] and spectrum analysis[6] because of its unique spectrum characteristics and parameter performances; it is one of the research hotspots of the ultrafast fiber laser in recent years.

At present, the commonly used method to obtain a laser pulse in this band is mainly based on nonlinear frequency transformation[7–10], such as soliton self-frequency shift (SSFS) and self-phase modulation (SPM), but the frequency shift often depends on the peak power of the pump pulse, which causes the output pulse frequency to be unstable. In addition, the laser output of the corresponding band can be directly achieved by pumping special doped ion fibers[11–13], such as bismuth-doped fiber, holmium-thulium co-doped fiber and thulium-terbium co-doped fiber. However, because these fibers containing special doped ions are still in the initial stage of research, the gain efficiency is low and they are too expensive to put into real commercial applications. In recent years, since thulium-doped fiber has a wide emission spectrum in the band of 1600–2100 nm, it has been used as an ideal medium to generate laser pulses in this band[14–17], but it is usually necessary to add photonic crystal fiber or dispersion-compensated fiber filters in the cavity to suppress long-wave emission.

Correspondence to: J. Zhang and M. Hu, Ultrafast Laser Laboratory, Key Laboratory of Optoelectronic Information Technology, Ministry of Education, School of Precision Instrument and Optoelectronics Engineering, Tianjin University, Tianjin 300072, China. Emails: zhangjiaxuan@tju.edu.cn (J. Zhang); huminglie@tju.edu.cn (M. Hu)

As a new laser technology that can generate special wavelength lasers, the Raman fiber laser has been widely considered in recent years. However, most of these lasers are based on continuous wave (CW) systems[18,19]. Equivalent saturable absorber mode-locking[20] is an effective method to obtain an ultrashort Raman pulse. However, this method requires longer Raman fiber to provide sufficient gain, which not only limits the repetition frequency of the system, but also increases the accumulation of intracavity dispersion and nonlinear phase shift, making the pulse transmission unstable and easily split. In recent years, with the development of techniques such as synchronous pump amplification[21–23], ultrashort pulse Raman fiber lasers have been developed rapidly, but it is necessary to ensure that the length of the Raman resonance matches the repetition rate of the pump pulse, and additional optical schemes are required to provide a coherent seed pulse for Raman amplification, which increases the complexity of the system. Besides, random distributed feedback[24–27] is also a novel method to generate an ultrashort Raman pulse, but requires a complex feedback control loop to match the pump repetition rate and the length of the Raman cavity in real time, and the output Raman spectrum not only inherits the noise of the pump laser, but also generates additional noise; thus, it shows a higher relative intensity noise (RIN).

In this paper, we propose and demonstrate a novel technique named coherent Raman amplification that can generate the NIR-III window ultrashort pulse directly without an additional seed in polarization-maintaining double-clad erbium-ytterbium co-doped fiber (PM-DC-EYDF). The numerical simulation results reveal the nonlinear dynamic process of the coherent Raman amplification in active fiber. The Raman gain is non-resonant and exists through the entire transparent region of the fiber; besides, no additional optical structure is needed to provide the seed source, and the self-seed can be generated by 1.5 μm pump laser pulse through nonlinear effects such as SPM and Raman scattering, thus reducing the complexity of the system. Finally, we simultaneously obtain an amplified 1.5 μm pump laser and NIR-III Raman pulses with the average power at the watts level by coherent Raman amplification and frequency shift through the experiment. The Raman pulse width can be compressed to 85 fs, which is the shortest pulse width of the NIR-III window obtained by gain fiber as far as we know.

2. Numerical analysis and simulation results

In order to obtain the high-energy NIR-III Raman laser pulse, we first research the principle of coherent Raman amplification and frequency shift in gain-regulated active fiber from the perspective of nonlinear dynamics.

As shown in Figure 1, it works like the Mamyshev oscillator[28–30] we are familiar with, which first broadens the spectrum by SPM and, when it reaches a sufficient width, the limited Raman gain band will act as a narrow band filter, filtering out the incompressible part of the spectrum. The gain in a certain spectrum range can be obtained by doping rare earth ions (erbium ions and ytterbium ions) into the fiber, so that the wavelength-shifted coherent Raman soliton can be electively amplified when transmitting in the active fiber. This hypothesis is based on the principle that the most coherent part of the SPM broadened spectrum shifts first in the frequency domain.

Based on the modified nonlinear Schrödinger equation[31,32], we explore the theoretical numerical model of wavelength-shifting soliton amplification in erbium-ytterbium co-doped fiber (EYDF). Except for the SPM, the equation also considers the spectrum evolution in the presence of spontaneous Raman scattering and gain:

$$\frac{\partial A}{\partial z}=\frac{g}{2}A+\sum_{n\geq 2}^{\infty}\frac{i^{n-1}}{i^{n}}\beta_n\frac{\partial^n A}{\partial T^n}+i\gamma\left(1+\frac{i}{\omega_0}\frac{\partial}{\partial T}\right)\times\left[(1-f_{\mathrm{R}})A|A|^2+f_{\mathrm{R}}A\int_0^{\infty}h_{\mathrm{r}}(\tau)|A(T-\tau)|^2\mathrm{d}\tau+iA\Gamma(T,z)\right], \tag{1}$$

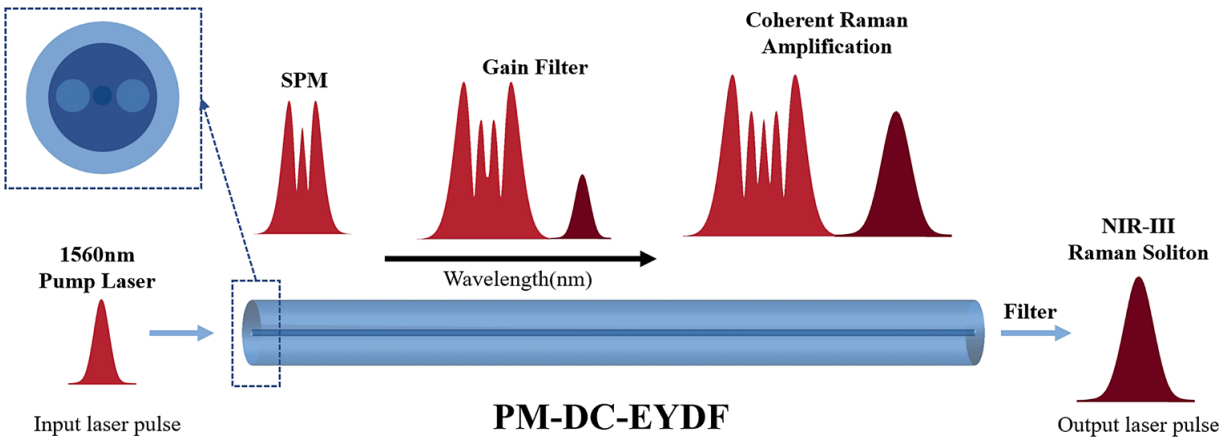

Figure 1. Schematic diagram of coherent Raman amplification.

https://doi.org/10.1017/hpl.2024.82 Published online by Cambridge University Press

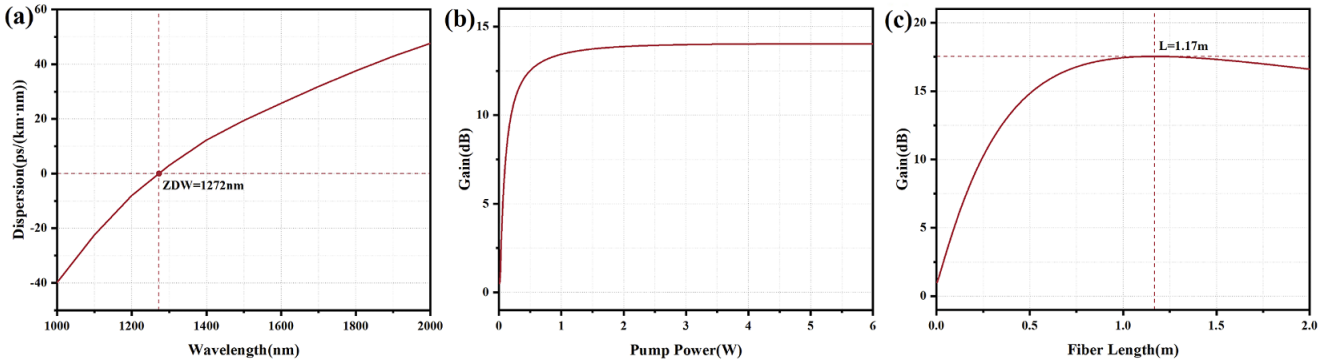

Figure 2. (a) The dispersion curve of the PM-DC-EYDF. The relationship between gain and (b) pump power and (c) fiber length.

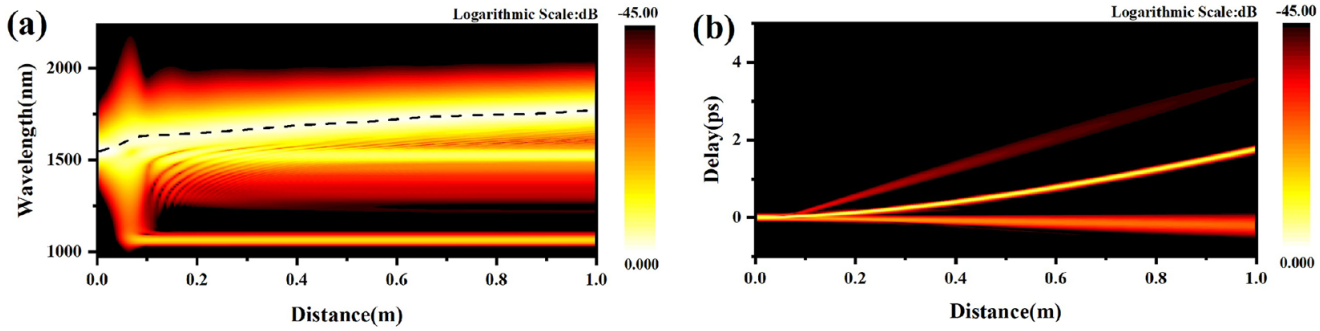

Figure 3. Simulation evolution diagram of (a) the frequency domain and (b) time evolution.

where g is the saturation gain coefficient, which is related to the small signal gain g_0 and can be expressed by the formula $g = g_0\left(1 + W_{\mathrm{P}}/W_{\mathrm{sat}} + (\omega-\omega_0)/\Delta\omega^2\right)$, W_{P} and W_{sat} denote the laser power and the gain saturation power, respectively, ω and ω_0 are the optical angular frequency and the central angular frequency, respectively, and $\Delta\omega$ is the gain bandwidth. Further, β_n denotes the nth-order dispersion coefficient associated with the Taylor series expansion of the propagation constant $\beta(\omega)$, which is related to the carrier frequency ω_0. In this paper, we only consider β_2, which represents group velocity dispersion (GVD), and β_3, which represents third-order dispersion (TOD):

$$\langle \Gamma(\omega,z)\ \Gamma^*\left(\omega',z'\right)\rangle = \frac{2f_{\mathrm{R}}\hbar\omega_0}{\gamma}\left|\mathrm{Im}\left[h_{\mathrm{r}}(\omega)\right]\right|\left[n_{\mathrm{th}}(|\omega|) + U(-\omega)\right]\times\delta\left(\omega-\omega'\right)\delta\left(z-z'\right). \quad (2)$$

The spontaneous Raman scattering term $\Gamma(T,z)$ is related to the Raman gain spectrum $\mathrm{Im}[h_{\mathrm{r}}(\omega)]$ and the boson factor $n_{\mathrm{th}}(\omega) = \left[\exp\left(h\omega/2\pi k_{\mathrm{B}}T\right)^{-1}\right]^{-1}$, where T is the temperature in kelvins and k_{B} is the Boltzmann's constant. Further, $U(\omega)$ is a step function.

We choose the simulation parameters according to the actual situation, and the PM-DC-EYDF is used as the gain fiber. The detailed dispersion curve of the fiber is shown in Figure 2(a), in which when the wavelength is more than 1272 nm, the fiber exhibits anomalous dispersion. The value is about 22 ps/(km·nm) at 1560 nm, that is, the corresponding parameter $\beta_2 = -28\ \mathrm{ps}^2/\mathrm{km}$. The seed source is a Gaussian ultrashort pulse laser with 20 nm spectrum width.

Figure 2(b) shows the relationship between the calculated gain of the PM-DC-EYDF and the average output power of the 976 nm CW pump source. When the pump power is low, the gain increases exponentially with the increase in the pump power. However, the curve gradually tends to be flat when reaching a threshold, indicating that the gain basically reaches saturation. In addition, we simulate the relationship between the signal gain and the fiber length when the pump power is set to 4 W. From the simulation shown in Figure 2(c), we can see that, at the given pump power, the signal gain is related to the fiber length; when the fiber length is less than 1.17 m, the gain increases with the length of the fiber, because the pump power is not fully utilized. When the fiber length is more than 1.17 m, the gain decreases gradually with the increase of fiber length, that is, the pump efficiency decreases, which means that the signal light is absorbed instead of being amplified; therefore, we consider that the length of the fiber that can achieve the highest pump efficiency in this experiment is 1.17 m.

Figures 3(a) and 3(b) show the simulated spectrum and temporal evolution, respectively. Due to SPM, the initial spectrum is first symmetrically broadened near 1560 nm with the increase of 976 nm CW pump power. Because the wavelength of the 1560 nm pulse pump is located in the anomalous dispersion region of the PM-DC-EYDF, the

https://doi.org/10.1017/hpl.2024.82 Published online by Cambridge University Press

spectrum of the fundamental soliton gradually shifts to the long-wavelength band under the effect of SPM. Besides, we can see the soliton fission effect from the time evolution diagram. Because the group velocity of the long-wavelength pulse is lower in the anomalous dispersion region, the soliton pulse becomes slower in the time domain. In addition, it can be seen that the pulse width of the soliton remains constant during transmission, which is the characteristic of fundamental solitons. At the same time, the simulation also proves that the key to obtain the required laser band through the coherent Raman fiber amplifier is whether SPM can broaden the spectrum to the Raman gain band of that waveband.

3. Experimental setup

To verify the simulation results, we design and build an experimental setup based on coherent Raman amplification, as shown in Figure 4.

The pulse pump source used to produce the Raman pulse is a homemade erbium-doped fiber amplifier (EDFA) that can output a 69 MHz pulse at 1557 nm with the spectrum bandwidth of 20 nm; the pulse train and spectrum are shown in Figures 5(a) and 5(b), in which we set the average power of the pump pulse to 150 mW and then coupled it with the 976 nm CW pump laser to the fiber. Before Raman amplification, we provide a pre-chirp for the pump pulse and the pulse width can be compressed to 300 fs by the grating pair (GP); the autocorrelation trace is shown in Figure 5(c). By adjusting the pulse width and the pump pulse energy, the spectrum can be broadened to the long wavelength under SPM at the beginning of fiber, and then the long-band spectrum can be used as the seed source by transmitting energy to the Raman pulse through coherent Raman scattering. Thus, we expect to obtain the ultrashort pulse laser output in the NIR-III region without injecting an additional long-wavelength seed.

Considering the group velocity mismatch between the amplified Raman pulse and the pump pulse, we use a 1.2 m-long PM-DC-EYDF (IXF-2CF-EY-PM-12-125, from iXblue) with the core diameter of 12 μm to realize Raman amplification, and the core absorption at 1536 nm is 65 dB/m. The gain distribution is wavelength-dependent and its dispersion curve is shown in Figure 2(a) where the zero-dispersion wavelength is located at 1272 nm. In order to restrain the parasitic laser, all the ends of the fiber are polished at the 8° angle. Finally, we use a long-pass filter (LPF) with the cut-off wavelength of 1600 nm to obtain

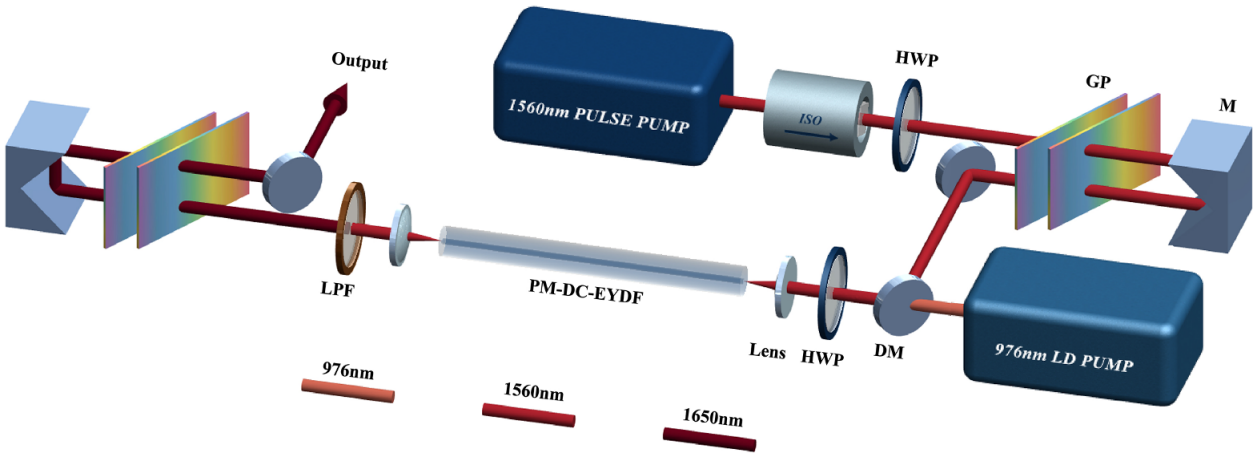

Figure 4. Schematic diagram of the coherent Raman amplification laser device. ISO, isolator; HWP, half wave plate; DM, dichroic mirror; GP, grating pair; LD, laser diode; LPF, long-pass filter; M, mirror.

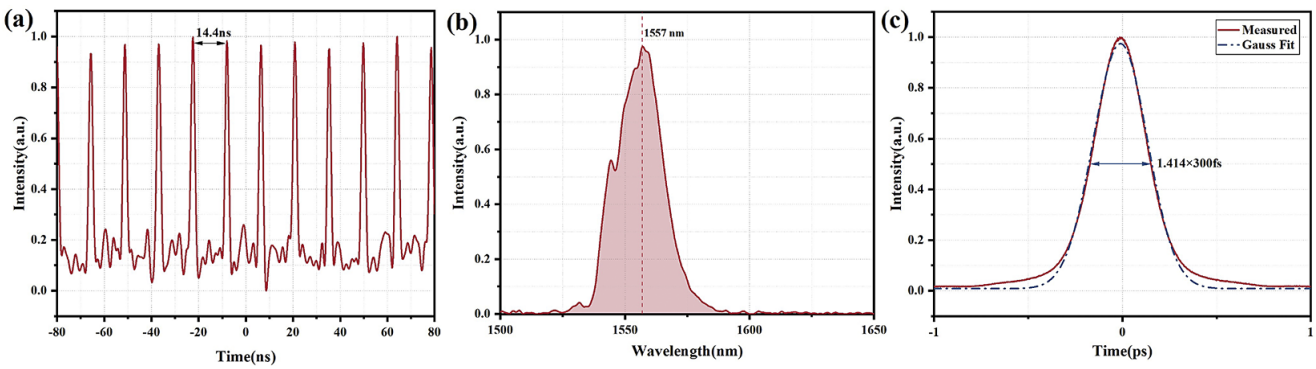

Figure 5. (a) Pulse train, (b) spectrum and (c) autocorrelation trace of the pump pulse.

https://doi.org/10.1017/hpl.2024.82 Published online by Cambridge University Press

the relatively pure Raman spectrum and the other GP to recompress the pulse width. Because stimulated Raman scattering (SRS) can provide a broad bandwidth and smooth gain in silica fiber, this method is expected to provide a sub-femtosecond pulse with high pulse energy after compression.

4. Experimental result and discussion

In this experiment, there will be some energy loss when entering the fiber, because the pump light uses the spatial coupling with the coupling efficiency of only 70%. Then, different degrees of optical gain can be generated by adjusting the power of the 976 nm pump source coupled to the fiber.

Figures 6(a) and 6(b) respectively show the spectrum evolution process before and after spatial filtering at the end of the PM-DC-EYDF under different 976 nm pump powers. Besides, we also draw a three-dimensional (3D) diagram, as shown in Figure 6(c), to observe the spectrum evolution process more intuitively. By analyzing these figures, we can see that when the pump power is below 3 W, there is only obvious spectrum broadening caused by SPM, and the corresponding power is too low to produce a spectrum in the Raman gain band (at around 1650 nm in this experiment). When the pulse power is higher than 3 W, the corresponding peak power can reach the threshold for generating the Raman gain, and the spectrum in this range will be amplified by SRS while, at the same time, the 1.5 μm pulse is also amplified by the 976 nm pump. Further increasing the pump power, the growth of the first-order Raman pulse begins to slow down, even appearing to have some loss and we determine that the second-order Raman pulse is generated; however, due to the limitation of the optical spectrum analyzer (OSA), we do not measure it this time.

Figure 6(d) shows the filtered Raman spectrum obtained at different pump powers (the right-hand edge is the noise wave caused by the OSA). It can be seen that the central wavelength of the output Raman pulse may shift with the change of the pump power. When the pump power is 3.5 W, the spectrum center wavelength is about 1675 nm and the spectral width is about 28 nm. The frequency difference between the first-order Raman pulse and the pump pulse is 13.2 THz, which accords with the standard value of Raman frequency shift of silica fiber. Finally, the pulse width can be compressed to 148 fs by the GP; the measured autocorrelation trace and the Gaussian fitted curve are shown in Figure 6(e). In addition, we also test the radio-frequency spectrum of the output Raman pulse, as shown in Figure 6(f). The peak occurs at 69.3 MHz, corresponding to the pulse train diagram in Figure 5(a). At the same time, the signal-to-noise ratio we measured is 55 dB, which proves that the laser system has good stability.

The relationship between the total output power and filtered Raman laser power with the pump power is shown in Figure 6(g). When the pump power is 4.5 W, the overall output power is 860 mW and the maximum average power of the first-order Raman pulse is 243 mW, which shows that our system can obtain a Raman pulse with 3.52 nJ energy. The reason for the low conversion efficiency is that, on the one hand, the input pump power is used to amplify the Raman pulse and, on the other hand, it is also consumed by the soliton frequency shift; in addition, there is also a part for the amplification of the 1.5 μm pump light. So, finally, we can obtain both the NIR-III Raman pulse and the amplified 1.5 μm pump pulse. We also test the power stability of the output Raman spectrum at the pump power of 3.5 W, as shown in Figure 6(h), in which the power is kept in a small fluctuation range during the 5 h monitoring period, and the root mean square (RMS) is 0.42%, so we conclude that the stability of the generated Raman laser pulse in this band is good.

In order to obtain higher energy Raman pulse output, we set the power of the 1.5 μm pulse pump to 270 mW, while increasing the length of the PM-DC-EYDF to 3 m, and obtain the spectrum evolution diagram as shown in Figure 7(a). It can be seen from the figure that the experimental results are similar to those in 1 m long EYDF. In the case of low power, the spectrum is first broadened by SPM and, when the pump power reaches the threshold of generating Raman gain, we can obtain the first-order Raman laser by coherent Raman scattering. The laser with wavelength over 1600 nm can be further filtered out through the filter, as shown in the Figure 7(b), and the spectrum width of the output near-infrared band can reach 58 nm, which means that the transformation limit pulse width can be narrower. The measured autocorrelation trace and Gaussian fitting curve are shown in Figure 7(c), where the pulse width can be 85 fs, which is the shortest pulse width of the NIR-III window obtained by gain fiber. The time–bandwidth product obtained in this work is about 0.543, and the reason why the pulse width is not compressed to the transformation limit is that the dispersion and nonlinear effects cause chirps when the pulse is transmitted in a transparent medium. As shown in Figure 7(d), when the pump power is 26 W, the output power before and after filtering is 1.92 and 1 W, respectively. That is, the obtained Raman pulse energy is 14.5 nJ. This means that coherent Raman amplification is an effective technique for obtaining high-energy ultrashort pulses.

From the above experiments, it can be seen that the generated Raman pulse is greatly affected by the 1.5 μm pump pulse, so we observe the effect on the generated Raman pulse by adjusting the pulse width and average power of the 1.5 μm pump. As shown in Figure 8(a), with the increase of pump pulse duration, the width of the obtained Raman pulse will gradually increase and the power conversion efficiency will decrease. This means that a narrower pump pulse width is more conducive to obtain high-energy femtosecond coherent

https://doi.org/10.1017/hpl.2024.82 Published online by Cambridge University Press

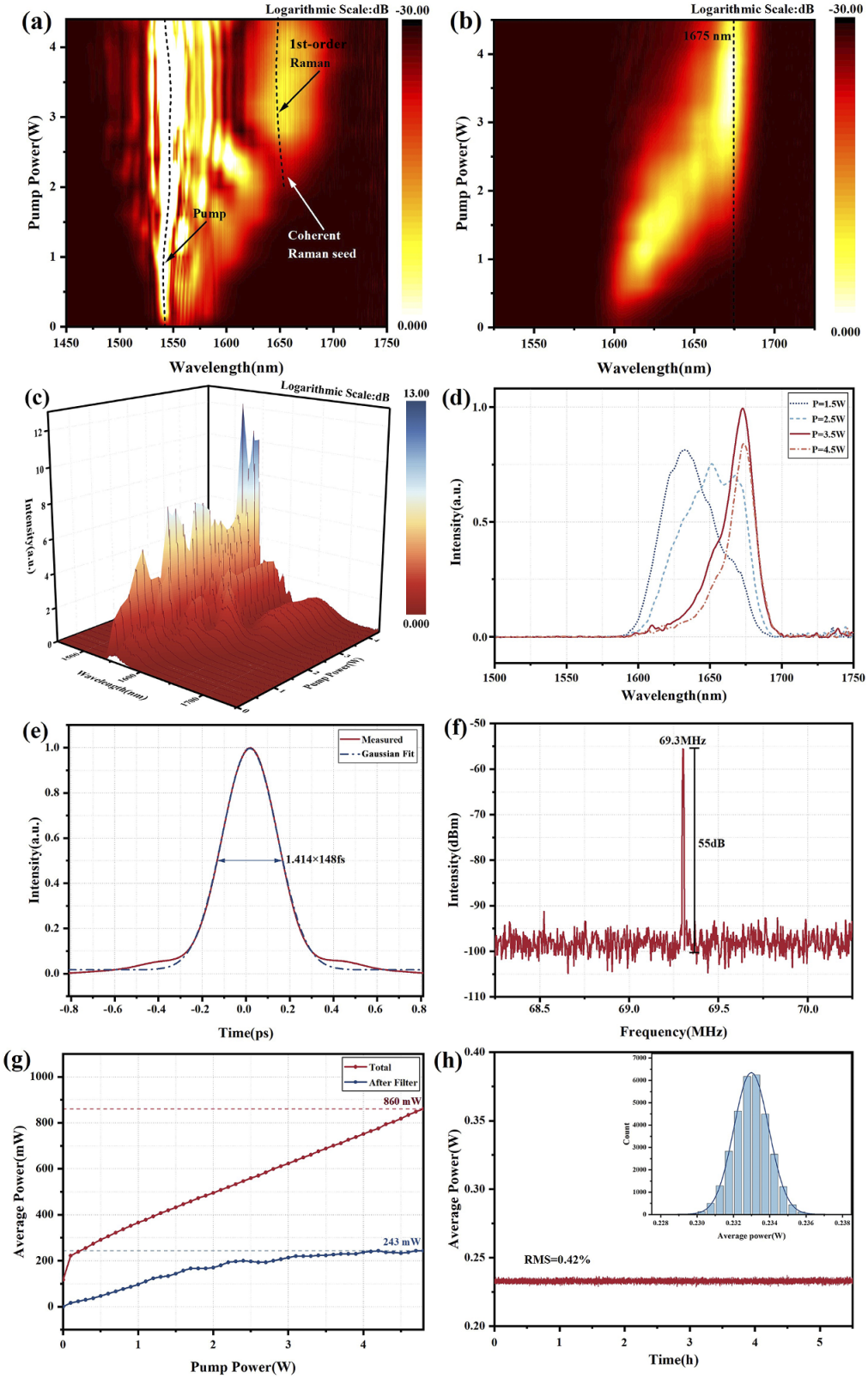

Figure 6. Schematic diagram of spectrum evolution (a) before and (b) after filtering. (c) 3D diagram of the spectrum evolution. (d) Raman spectrum when the pump power is 1.5 W (dot line), 2.5 W (dash line), 3.5 W (solid line), 4.5 W (dot dash line), respectively. (e) Measured autocorrelation trace and Gaussian fitting curve when the pump power is 4.5 W. (f) Radio-frequency spectrum of the Raman pulse. (g) Variations in the total output power and filtered Raman pulse power with the pump power. (h) Raman laser power fluctuation test curve with time.

https://doi.org/10.1017/hpl.2024.82 Published online by Cambridge University Press

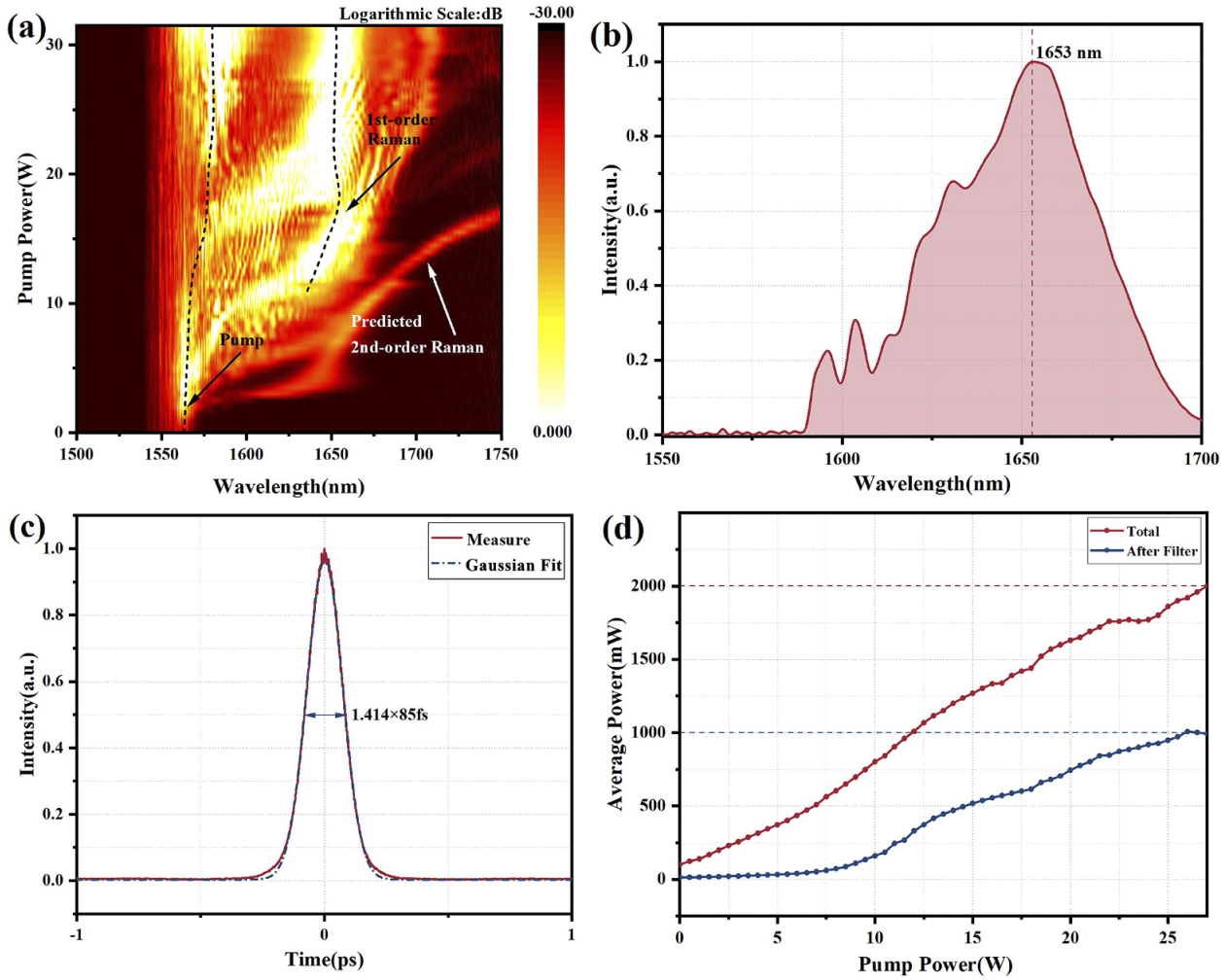

Figure 7. (a) Total spectrum evolution diagram in 3 m PM-DC-EYDF. (b) When the pump power is 9 W, measured Raman spectrum after filtering and (c) measured autocorrelation trace and Gaussian fitting curve. (d) Variations in the total output power and filtered Raman laser power with the pump power in 3 m PM-DC-EYDF.

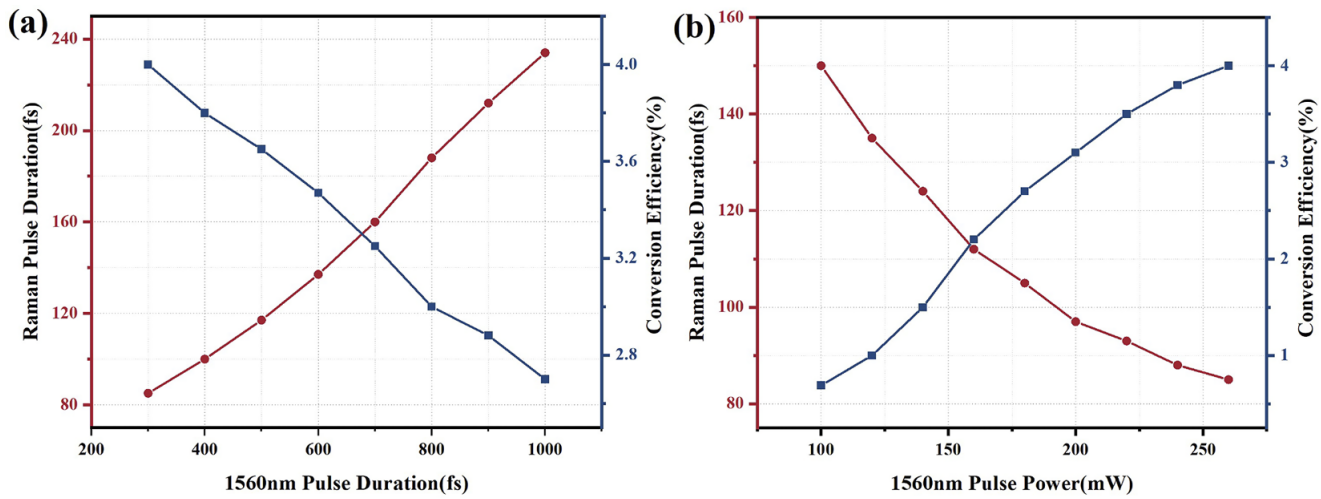

Figure 8. Variations in Raman pulse duration (circular point) and conversion efficiency (square point) with (a) pulse duration and (b) power of the 1560 nm pump.

https://doi.org/10.1017/hpl.2024.82 Published online by Cambridge University Press

Raman pulses. After that, we set the pump pulse width to 300 fs and observe the curve of the Raman pulse width and conversion efficiency changing with the 1.5 μm pump power, as shown in the Figure 8(b). We can see that, as the input pump power increases, the conversion efficiency gradually increases, while the output Raman pulse duration becomes narrower; therefore, we can predict that the Raman pulse with better performance can be obtained by using the pump pulse with narrower pulse durations and higher power.

This paper proves that we can obtain an NIR-III laser in the PM-DC-EYDF through coherent Raman amplification technology. In addition, it has been experimentally demonstrated that this nonlinear dynamic process also exists in the polarization-maintaining ytterbium-doped fiber (PM-YDF), which can achieve coherent Raman amplification from 1.06 to 1.1 μm[33]. Besides, the numerical simulation results show that the theory is also applicable to passive fiber without ion doping; however, it should be noted that due to the lack of CW pumping in the passive fiber, the noise characteristics of the Raman pulse are mainly determined by the pulse pump source; therefore, it is necessary to select a pulse pump source with low RIN for Raman amplification in order to obtain a more stable Raman laser output. This means that the nonlinear effect is not a special phenomenon of a particular fiber, but rather a basic characteristic of many kinds of fibers. In addition, the Raman frequency shift is mainly determined by the material of the fiber.

5. Conclusion

In conclusion, we adopt coherent Raman amplification in this paper to realize the 1560 nm pump pulse frequency shift to the NIR-III window, and achieve the amplification of the Raman pulse at the same time. The system structure is simple and the Raman laser in the 1600–1700 nm band can be output by adjusting the input pump power without the injection of an additional seed source pulse in the near-infrared band. Finally, we obtain a watt-level first-order Raman pulse with the central wavelength of 1650 nm, and the pulse width is 85 fs. It is enough to meet the detection requirements in biomedical imaging, laser precision machining and other fields. In addition, we demonstrate that a high-energy narrow pulse seed source is more conducive to the generation of high-quality Raman pulses. This method can be used in all kinds of fibers, and is expected to be a widely used ultrafast fiber laser technology.

Acknowledgements

The authors wish to acknowledge Wei Chen and Jintao Fan for their very valuable discussions. This work was supported by the National Natural Science Foundation of China (Grant No. 62227821) and the National Key Research and Development Program of China (Grant Nos. 2022YFF070600 and 22023YFB3611000).

References

1. C. Kerse, H. Kalaycioglu, P. Elahi, B. Cetin, D. K. Kesim, O. Akcaalan, S. Yavas, M. D. Asik, B. Oktem, H. Hoogland, R. Holzwarth, and F. O. Ilday, Nature **537**, 84 (2016).
2. N. G. Horton, K. Wang, D. Kobat, C. G. Clark, F. W. Wise, C. B. Schaffer, and C. Xu, Nat. Photonics **7**, 205 (2013).
3. E. Agrell, M. Karlsson, F. Poletti, S. Namiki, X. Chen, L. A. Rusch, B. Puttnam, P. Bayvel, L. Schmalen, Z. N. Tao, F. R. Kschischang, A. Alvarado, B. Mukherjee, R. Casellas, X. Zhou, D. vanVeen, G. Mohs, E. Wong, A. Mecozzi, M. S. Alouini, E. Diamanti, and M. Uysal, J. Opt. **18**, 063002 (2016).
4. S. P. Chong, C. W. Merkle, D. F. Cooke, T. W. Zhang, H. Radhakrishnan, L. Krubitzer, and V. J. Srinivasan, Opt. Lett. **40**, 4911 (2015).
5. M. Yamanaka, T. Teranishi, H. Kawagoe, and N. Nishizawa, Sci. Rep. **6**, 31715 (2016).
6. C. Li, J. W. Shi, X. J. Gong, C. H. Kong, Z. C. Luo, L. Song, and K. K. Y. Wong, Opt. Lett. **43**, 5849 (2018).
7. K. Wang and C. Xu, Appl. Phys. Lett. **99**, 071112 (2011).
8. T. N. Nguyen, K. Kieu, D. Churin, T. Ota, M. Miyawaki, and N. Peyghambarian, IEEE Photonics Technol. Lett. **25**, 1893 (2013).
9. P. Cadroas, L. Abdeladim, L. Kotov, M. Likhachev, D. Lipatov, D. Gaponov, A. Hideur, M. Tang, J. Livet, W. Supatto, E. Beaurepaire, and S. Fevrier, J. Opt. **19**, 065506 (2017).
10. H. Y. Chung, W. Liu, Q. Cao, F. X. Kärtner, and G. Q. Chang, Opt. Express **25**, 15760 (2017).
11. T. Noronen, O. Okhotnikov, and R. Gumenyuk, Opt. Express **24**, 14703 (2016).
12. T. Noronen, S. Firstov, E. Dianov, and O. G. Okhotnikov, Sci. Rep. **6**, 24876 (2016).
13. A. Khegai, M. Melkumov, K. Riumkin, V. Khopin, S. Firstov, and E. Dianov, Opt. Lett. **43**, 1127 (2018).
14. J. X. Chen, X. Y. Li, T. J. Li, Z. Y. Zhan, M. Liu, C. Li, A. P. Lou, P. Zhou, K. K. Y. Wong, W. C. Xu, and Z. C. Luo, Photonics Res. **9**, 873 (2021).
15. J. X. Chen, Z. Y. Zhan, C. Li, M. Liu, A. P. Luo, P. Zhou, W. C. Xu, and Z. C. Luo, Opt. Lett. **46**, 3637 (2021).
16. S. X. Chen, Y. H. Chen, K. Liu, R. Sidharthan, H. Z. Li, C. J. Chang, Q. J. Wang, D. Y. Tang, and S. Yoo, Opt. Lett. **46**, 5922 (2021).
17. Z. W. Lin, J. X. Chen, T. J. Li, Z. Y. Zhan, M. Liu, C. Li, A. P. Lou, P. Zhou, W. C. Xu, and Z. C. Luo, Opt. Express **30**, 32347 (2022).
18. C. Headley and G. P. Agrawal, *Raman Amplification in Fiber Optical Communication Systems* (Elsevier, 2005).
19. M. N. Islam, IEEE J. Sel. Topics Quantum Electron. **8**, 548 (2002).
20. A. Chamorovskiy, J. Rautiainen, J. Lyytikäinen, S. Ranta, M. Tavast, A. Sirbu, E. Kapon, and O. G. Okhotnikov, Opt. Lett. **35**, 3529 (2010).
21. C. Finot, G. Millot, C. Billet, and J. M. Dudley, Opt. Lett. **11**, 1547 (2003).
22. C. Finot, G. Millot, S. Pitois, C. Billet, and J. M. Dudley, IEEE J. Sel. Top. Quantum. **10**, 1211 (2004).
23. M. Hardy, M. Olivier, and M. Piché, J. Opt. Soc. Am. B **32**, 1593 (2015).
24. W. Pan, L. Zhang, H. Jiang, X. Yang, S. Cui, and Y. Feng, Laser Photonics Rev. **12**, 1700326 (2018).

https://doi.org/10.1017/hpl.2024.82 Published online by Cambridge University Press

25. S. K. Turitsyn, S. A. Babin, A. E. El-Taher, P. Harper, and E. V. Podivilov, Nat. Photonics **4**, 231 (2010).
26. Z. N. Wang, Y. J. Rao, H. Wu, P. Y. Li, Y. Jiang, X. H. Jia, and W. L. Zhang, Opt. Lett. **20**, 17695 (2012).
27. L. Zhang, H. Jiang, X. Yang, W. Pan, and Y. Feng, Opt. Lett. **41**, 215 (2016).
28. P. V. Mamyshev, in 24*th European Conference on Optical Communication* (IEEE, 1998.), p. 475.
29. J. C. Zheng, Y. Song, K. Y. Lau, and L. Li, Opt. Fiber Technol. **67**, 102691 (2021).
30. W. Stepien and J. R. Marciante, J. Opt. Soc. Am. B **39**, 626 (2022).
31. S. Lefrancois and F. Wise, in *CLEO: Science and Innovations 2011* (Optica, 2011), paper CThU2.
32. F. X. Kartner, D. J. Dougherty, and H. A. Haus, J. Opt. Soc. Am. B **11**, 1267 (1994).
33. C. Wei, Z. W. Xu, A. C. Ge, Y. J. Gao, J. T. Fan, H. Y. Song, B. W. Liu, J. Y. Li, C. Y. Wang, and M. L. Hu, J. Lightwave Technol. **36**, 5237 (2018).

https://doi.org/10.1017/hpl.2024.82 Published online by Cambridge University Press